Research Article | Vol. 30, No. 13 / 20 Jun 2022 / Optics Express 23163
Optics EXPRESS

Performance investigation of high-efficiency widely tunable subnanosecond optical parametric generator and amplifier based on MgO:PPLN

JONAS BANYS,* JUSTINA SAVICKYTĖ, ONA BALACHNINAITĖ, SIMONA ARMALYTĖ, VIKTORIJA TAMULIENĖ, VYGANDAS JARUTIS, AND JULIUS VENGELIS

Laser Research Center, Vilnius University, Sauletekio Ave. 10, Vilnius LT 10223, Lithuania
jonas.banys@ff.vu.lt

Abstract: We report on experimental and theoretical studies of widely tunable high-efficiency subnanosecond optical parametric generator (OPG) and amplifier (OPA) based on a 2 cm long multigrating MgO-doped periodically-poled lithium niobate (MgO:PPLN) crystal pumped by a passively Q-switched Nd:YAG micro-laser. Our OPG can be continuously tuned from 1442 nm to 4040 nm with signal wave energies ranging from 33 μJ to 265 μJ and total OPG conversion efficiency up to 46 % that depended on the pump focusing conditions. Characterization of spatial properties of the OPG determine Lorentzian spatial profile of the signal beam with $M^2 \approx 2$ that was also dependent on the pump focusing conditions. High OPG gain and subsequent pump depletion led to the adjustment of the output signal pulse duration in the range of 242 – 405 ps by varying the incident pump power. By using a distributed feedback (DFB) continuous-wave (CW) 1550 nm wavelength seed laser for the OPA operation we reduced the generation threshold up to 1.6 times, increased maximum conversion efficiency by 4 – 20%, and achieved nearly transform-limited output signal pulses. Experimentally measured characteristics were supplemented by numerical simulations based on the quantum mechanical model for the OPG, and classical three-wave interaction model for the OPA operation.

1. Introduction

For continuously tunable coherent light in the wide spectral ranges, the optical parametric generator (OPG) has the advantages of a simple construction and a flexible tuning technique. Compact size low cost widely tunable subnanosecond (100 ps - 1 ns) OPGs are attractive for various applications where high temporal resolution supplied by expensive and sophisticated ultrashort (<10 ps) laser systems is not required but meanwhile the nanosecond (>1 ns) temporal resolution is insufficient. The main areas where these devices could be applied include spectroscopy [1,2], gas detection [3,4], remote target detection [5], biological studies [6,7], as pumping beams for the nonlinear-frequency-conversion generation of terahertz waves [8] and other areas. However, even in the case of high demand for such devices and high technological progress of high energy compact Q-switched microchip lasers used for pumping, subnanosecond OPG's are still not widely developed. The main challenge in creating this type of device is the laser induced damage threshold (LIDT) of nonlinear media, which for many nonlinear materials is lower than the threshold of optical parametric generation for subnanosecond pulses. Coupled to quasi-phase-matched (QPM) [9] nonlinear optical materials with the highest nonlinearity, a passively Q-switched microchip Nd:YAG laser can be an efficient pump source for producing tunable subnanonsecond laser radiation through parametric light generation. For the first time in 1997, single-frequency l-ns pulse duration passively Q-switched microchip laser has been

#459826 https://doi.org/10.1364/OE.459826
Journal © 2022 Received 18 Apr 2022; revised 25 May 2022; accepted 26 May 2022; published 9 Jun 2022

Optics EXPRESS

used to drive periodically-poled lithium niobate (PPLN) optical parametric amplifiers (OPA), producing 100-kW subnanosecond pulses at wavelengths between 1.4 and 4.3 μm with total conversion efficiency of 25% [10]. Chiang *et al.* showed the generation of a subnanosecond visible laser radiation by using a second harmonic generation (SHG) and OPG cascaded process in monolithic 30-mm-long PPLN pumped by a 730-ps passively Q-switched Nd:YAG laser with the total OPG conversion efficiency of 26% [11]. H. Ishizuki *et al.* demonstrated mid-infrared OPG based on MgO:PPLN and pumped by a low repetition rate subnanosecond microchip laser with the maximum total output energy of 1 mJ and 40 % conversion efficiency [12]. Yue *et al.* [13] reported a MgO:PPLN OPG with 1.0-mJ single pulse energy, 390-ps pulse width, 2.6-MW peak power, and 100-Hz repetition rate at 1560 nm pumped an Nd:YAG/Cr:YAG microlaser, but the conversion efficiency was quite limited. Subnanosecond microlaser pumped 40-mm-long MgO:PPLN based OPG, seeded with a distributed feedback continuous-wave (CW) diode laser, was demonstrated by Liu *et al.* [14]. The OPG achieved a quantum conversion efficiency of 61.2% and a slope efficiency of 41.8% but the signal tuning range was narrow (from 1651.0 to 1652.4 nm). In [15] high efficiency subnanosecond OPG based on multigrating 50-mm-long MgO:PPLN crystal with the MW level output peak power and total conversion efficiency of 67.16 % was presented. Recently, Zhong *et al.* demonstrated up to 47.9% efficient tunable subnanosecond OPG with its linewidth close to the Fourier transform limit by injection seeding with a tunable diode laser [16]. However to date, no subnanosecond OPGs based on short (up to 20 mm in length) periodically poled crystals have been demonstrated that can be both effective and continuously tunable over a wide spectral range. Extensive theoretical and experimental investigation of such OPGs is necessary in order to create a commercially attractive product.

In this paper, we thoroughly investigate widely and continuously tunable subnanosecond OPG based on multiperiod MgO:PPLN crystal with, to the best of our knowledge, the highest conversion efficiency for 20 mm length PPLN crystal. The OPG was continuously tunable over the range of 1442 – 4040 nm by changing the grating period and the temperature of the crystal. Pumped by a microchip passively Q-switched laser (520 ps pulse duration, 1 kHz pulse repetition rate) with a maximum average output power of 1 W, the OPG provided signal wave average powers of 23 – 265 mW whereas total conversion efficiency of 23 % to 46% was achieved and depended on the pump focusing conditions. The spectral bandwidth variation in the tuning process of OPG was calculated and measured, and the feasibility of broadband infrared laser output by OPG was discussed. Experimentally measured spatial and temporal characteristics of the signal wave were also shown. By injection-seeding with a narrow (<500 kHz) linewidth CW diode laser for OPA operation, the generation threshold and signal pulse linewidth were significantly decreased while conversion efficiency increased by 4 –20 %. The experimental data were supplemented by the results of numerical simulations. For OPG, the quantum mechanical model from [17] was adopted for the subnanosecond regime for the first time. The model allowed the estimation of signal spectra and provided the explanation for the dependence of the conversion efficiency to signal wave on the grating period. On the other hand, OPA theoretical model was based on the classical three-wave interaction equations that evaluated signal wave conversion efficiency, spectrum, and pulse profile.

2. Theoretical analysis of OPG in MgO:PPLN crystal

Here, we follow the formalism that was developed in [17], where the formula for OPG output signal spectrum as well as output power was derived. The formula is suitable for MgO:PPLN crystal. The Gaussian shapes were assumed for both pulse and beam profiles. The formula for the output signal energy of OPG reads:

$$E_1 = \int_{\omega_{s0}-\Delta\omega}^{\omega_{s0}+\Delta\omega} \int_{-\Delta\varphi_x}^{\Delta\varphi_x} \int_{-\Delta\varphi_z}^{\Delta\varphi_z} \int_{-\Delta t}^{\Delta t} \int_0^R W(\varphi_x, \varphi_z)\beta_s L^2 \frac{\sinh^2 B}{B^2} 2\pi r dr dt d\varphi_z d\varphi_x d\omega_s. \quad (1)$$

Optics EXPRESS

Let us shortly define the variables. First, $B = \sqrt{g^2 - \frac{\Delta k^2}{4}}L$, where the gain g and is defined as follows:

$$g^2 = \frac{2\omega_s\omega_i d_{\text{eff}}^2 I_p}{\varepsilon_0 n_s(\omega_s) n_i(\omega_i) n_{p0} c^3} F_r(r) F_t(t), \tag{2}$$

where $F_r(r) = \exp\left(-2\frac{r^2}{r_p^2}\right)$ and $F_t(t) = \exp\left(-4\ln 2\frac{t^2}{\tau_p^2}\right)$. The phase mismatch Δk is defined as

$$\Delta k = k_{p0} - k_g - k_s\cos\varphi_x\cos\varphi_z - \sqrt{k_i^2 - (k_s\sin\varphi_z)^2 - (k_s\sin\varphi_x\cos\varphi_z)^2}. \tag{3}$$

Here and further indexes s, i and p stand for the signal, idler and pump waves, respectively. Index 0 stands for the central wavelength or frequency. The scaling factor $\beta_s = [h\omega_s^3 n_s^2(\omega_s)/(4\pi^3 c^2)]g^2$. The weighting function

$$W(\varphi_x, \varphi_z) = \exp\left(-2\frac{\varphi_x^2 + \varphi_z^2}{\phi_{\text{diff}}^2}\right). \tag{4}$$

accounts experimentally observed fluorescence angles of the signal and is modeled through the diffraction angle $\phi_{\text{diff}} = \frac{\lambda_{p0}}{\pi r_p n_p}$. The other variables and parameters are described in Table 1. The vector diagram of the three-wave interaction is shown in Fig. 1, where k_{p0}, k_s, k_i, and k_g are the pump, signal, idler, and grating wave vectors. Outermost integral in Eq. (1) gives total generated energy and four internal integrals provide the OPG spectrum.

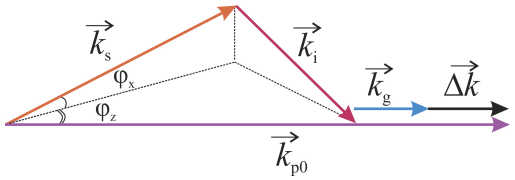

Fig. 1. Phase mismatch diagram. Adapted from [17].

Table 1. Description of variables and parameters

Variable	Description	Variable	Description	Parameter	Description	Value
r, R	radial coordinate, its limit value	k_g	grating wavevector	d_{eff}	nonlinear coefficient	17 pm/V
t, Δt	time, its limit value	n	refractive index	r_p	pump beam waist radius	80 μm
φ_x, φ_z	diffraction angles	c	speed of light	τ_p	pump pulse duration	520 ps
$\Delta\varphi_x$, $\Delta\varphi_z$	limit values of angles	h	Plank constant	L	crystal length	2 cm
ω, $\Delta\omega$	cyclic frequency, its limit value	I_p	peak pump intensity	λ_{p0}	pump wavelength	1064 nm
λ	wavelength	T	temperature			
k	wavenumber	Λ	grating period			

In Figs. 2,3 the theoretical results of subnanosecond OPG are presented. The Sellmeier equations for MgO:PPLN from [18] at type-0 (e→ee) interaction were utilized. Here, the grating period Λ and correspondingly grating wavevector $k_g = 2\pi/\Lambda$ were varied. From Eqs. (1)–(2) we may show that the conversion efficiency increases with the increase of the grating period due to two reasons. First, the signal frequency decreases when the grating period increases. As we can see from Eq. (2), the increment $g^2 \propto \omega_s\omega_i = \omega_{p0}^2(s - s^2)$, where $s = \omega_s/\omega_{p0}$ and $\omega_i = \omega_{p0} - \omega_s = \omega_{p0}(1 - s)$. Since the function $f(s) = s - s^2$ obeys a maximum at $s = 1/2$ (the

Optics EXPRESS

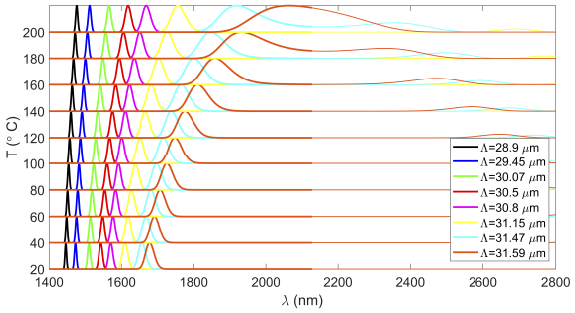

Fig. 2. Output signal spectra calculated from quantum mechanical model for 8 different grating periods and different crystal temperatures. Thin lines - idler wave. 70 mW pump power.

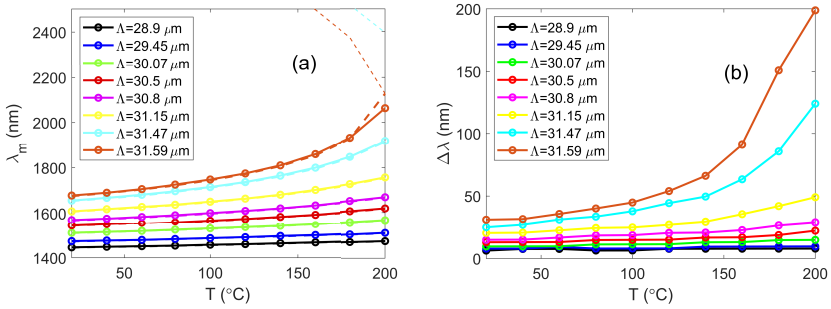

Fig. 3. Dependence of signal central wavelength (a) and spectral width (b) on temperature for different grating periods Λ. Dashed lines in (a): signal wavelengths calculated from QPM conditions. 70 mW pump power.

degenerate regime), the gain increment increases with the increase of the grating period. The second reason is the signal spectrum broadening at the degeneracy [19].

We note, that in this model, the conversion efficiency does not saturate – in Eq. (1), undepleted pump pulsed beam is assumed. The beam diffraction, limited MgO:PPLN transmission, and pulse dispersion effects are neglected as well. As a result, signal wave power permanently grows exponentially and at large gain increment and crystal length product (gL>10) values, Eq. (1) overestimates the signal generation threshold and power but estimates the signal spectrum well [17]. Therefore, here we present only the theoretical signal spectra, Fig. 2. We can see that the signal spectra shift to the longer wavelengths when the grating period increases.

Another possibility to vary the signal spectrum is the temperature tuning (Figs. 2, 3(a)). The numerically calculated signal wavelength at spectral maximum for different grating periods is shown in Fig. 3(a) (solid lines). Here, the dependence on the temperature is depicted. The dashed lines show the wavelengths which were calculated from the QPM condition. Continuous tuning range predicted from the model is wide and ranges from 1445 nm to 4040 nm. The actual wavelengths almost coincides with the theoretical (QPM) ones. From spectral FWHM dependence on crystal temperature (Fig. 3(b)) it can also be seen, that the spectrum width is larger for longer periods, increases with temperature and obeys the values over 20 nm for the grating periods Λ = 31.15 – 31.59 μm. At period value Λ = 31.59 μm, the degenerate regime can be achieved through the temperature tuning, which produces very broad, ≈200 nm FWHM, output spectra, see Fig. 2, T = 200 °C.

Optics EXPRESS

3. Experimental setup

Experimental setup for the subnanosecond OPG and OPA is shown in Fig. 4. Both OPG and OPA were pumped by passively Q-switched Nd:YAG MOPA microlaser (Standa Ltd) that generated up to 1 W average power subnanosecond (520 ps) 1064 nm wavelength pulses at 1 kHz pulse repetition rate. Measured pump beam quality parameter $M^2 = 1.3$. Half-wave plate placed on a motorized rotation stage together with a Brewster-type polarizer were used to attenuate the pulse energy and assure vertical polarization for pumping the OPG. The pump beam was directed to an adjustable beam expander (telescope). By using the telescope and the lens with a focal length of 250 mm the beam waist diameter ($1/e^2$ level) at the focusing point in the MgO:PPLN crystal could be varied. Hence the variation of pump focusing parameter is obtained, which is defined as $\xi = L/b$, where L is the crystal length and $b = 2z_R$ is the confocal parameter of the pump beam (z_R is the Rayleigh length) [20].

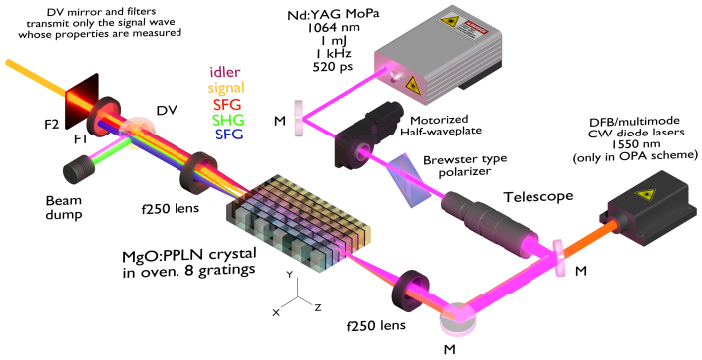

Fig. 4. Experimental setup of subnanosecond OPG (unseeded) and OPA (seeded) based on a MgO:PPLN crystal.

Periodically-poled MgO doped lithium niobate crystal was 20 mm long, 10 mm wide, and 1 mm height with 8 gratings of 28.9, 29.45, 30.07, 30.05, 30.8, 31.15, 31.47 and 31.59 μm periods. Facets of the crystal were anti-reflection coated for pump and OPG wavelengths. Crystal was placed into an oven that could be heated up to 200 °C using a temperature controller (HC Photonics) with a stability of 0.1 °C. The oven with the crystal was attached onto a three-axis (x, y, z) translation stage with additional possibility of tilting and rotation to adjust the crystal more precisely. In the experiments only OPG signal waves were registered. The wavelength tuning of OPG was realized by changing the temperature and the grating period. In the crystal not only the signal and idler waves were generated but also parasitic second harmonic (SHG, 532 nm) and two sum-frequency (SFG) wavelengths in red and blue spectral region were observed. All of the generated wavelengths except of signal were filtered down using different filters F1 (T>70% at 1526 – 2000 nm, T≈0.1% 200 – 1500 nm and 2 μm – 12 μm), F2 (T≈0.1% at 300 – 900 nm and T>80% at 1400 – 2700 nm) and dichroic mirror DV (R>99.5% at 1064 nm and 532 nm, T≈96% at 1400 – 2128 nm). Output signal spectra were measured using a NIRQuest512-2.5 (Ocean Insight) spectrometer which covers 0.9 μm – 2.5 μm spectral range with resolution of 6.5 nm (FWHM). The signal output power was measured using a thermopile based power meter 3A (Ophir). For the narrowing of the linewidth of the OPG signal the injection seeding was used converting the OPG configuration to an OPA. Two 1550 nm wavelength seed sources were used - a 1 mW power DFB CW diode laser with a linewidth of <500 kHz and a multimode diode laser (MDL). Seed beam was overlaped with the pump beam in the crystal using two positioning mirrors and the same focusing lens.

Optics EXPRESS

4. Experimental results and discussion

4.1. Power scaling characteristics

Average power scaling and OPG conversion efficiency are one of the key characteristics that describe the performance of the OPG. Figure 5 shows the dependence of the signal wave average power on the pump power for all 8 gratings. Here we describe two parametric generation cases based on the focusing parameter ξ – sharp pump beam focusing condition (beam waist diameter d_p ≈160 μm, ξ = 0.7), and a weak one (d_p ≈460 μm, ξ = 0.05). In the case of sharp focusing, the generation of signal pulses in the 1442 – 2128 nm spectral range was observed at a pump threshold of around 25 – 50 mW, which was defined by the detection of the output pulse power of 10 μW (power meter sensitivity limit). Generation threshold decreased with the increasing grating period as predicted from the Eqs. (1)–(2). Moreover, due to limited MgO:PPLN transmission, for the first two gratings idler wave (beyond 3.5 μm) is partially absorbed, hence we observe higher generation threshold. Since the OPG worked in a high-gain regime (gL = 16 – 29>>1), above the threshold, signal power (efficiency too) grew exponentially with the pump power which is consistent with the numerical calculations. As the pump is increased further, signal power starts to deviate from exponential growth since the pump pulse intensity is no longer constant due to its depletion. The effect of pump depletion is clearly visible as the curves from the signal conversion efficiency vs pump power graph (inset Fig. 5(a)) saturate with the increasing pump power. Nevertheless, at maximum pump power (100 mW), signal power reaches 26 – 33 mW which corresponds to high conversion efficiency of 26 – 33 %. Maximum output power is achieved with the longest grating period, which at MgO:PPLN temperature of 200 °C, resembles degenerate regime where signal and idler waves are indivisible. Long-term power stability measurements were also performed and signal output power was recorded to exhibit excellent stability: better than 0.3% rms over a period of 1 hour at the maximum pump power of 100 mW.

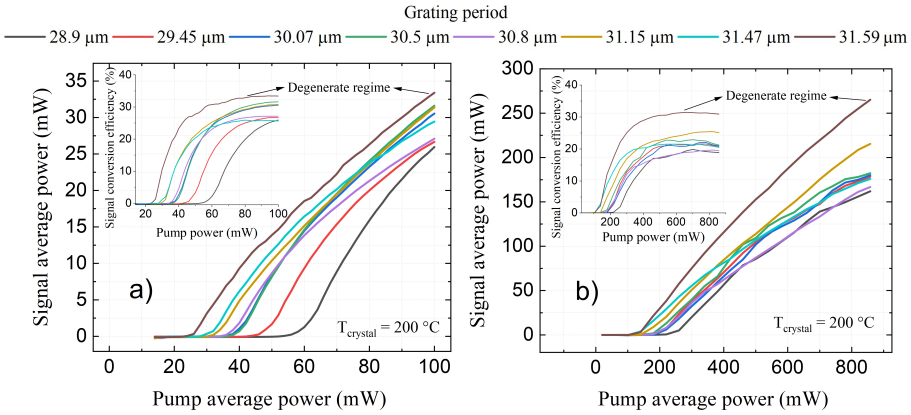

Fig. 5. Signal wave average power as a function of pump power for 8 gratings in OPG regime. Sharp (a) and weak (b) focusing conditions. Insets show signal conversion efficiency vs pump power. T = 200 °C.

In order to fully utilize the available pump power from the microlaser, we focused the pump beam very weakly (d_p ≈460 μm, ξ = 0.05). This allowed to extract almost one order of magnitude higher signal output powers (162 – 265 mW at 860 mW pump power) with 2 – 7 % lower efficiency (Fig. 5(b)). In both focusing cases, peak fluence in the MgO:PPLN was limited to ~1 J/cm^2 – this ensured optical damage-free crystal operation. Taking into account the idler wave (2490 – 4040 nm range), whose power has been calculated from Manley – Rowe relations, total conversion efficiency for all 8 gratings ranges from 23 % to 46 % (Fig. 6(a)). To the best of our

Optics EXPRESS

knowledge, these are the highest OPG efficiencies obtained from 2 cm long MgO:PPLN crystal in the subnanosecond regime.

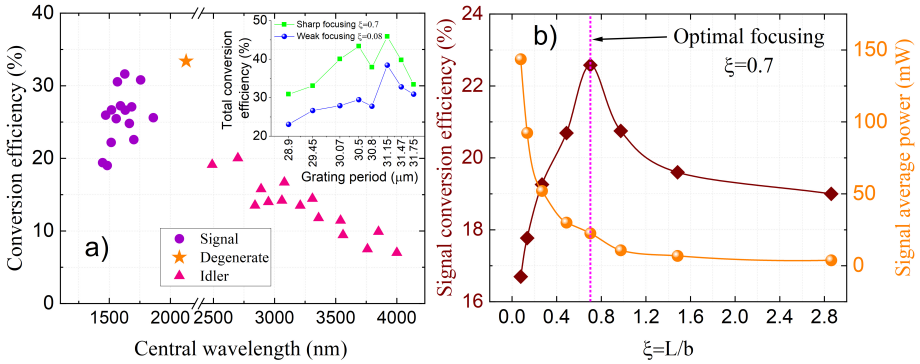

Fig. 6. OPG conversion efficiency distribution at different signal and idler wavelengths (a). Inset shows total OPG conversion efficiency as a function of grating period for sharp and weak focusing conditions. (b) – signal wave conversion efficiency and average power dependencies on pump focusing parameter ξ for a Λ = 31.59 μm grating (maximum fluence limited to 1 J/cm^2).

By varying pump beam waist diameter incident into a crystal, we measured signal wave average power and conversion efficiency as a function of the focusing parameter ξ (Fig. 6(b)) while limiting maximum fluence to 1 J/cm^2 (or peak intensity to ~2 GW/cm^2). Such graph represents optimal pump focusing conditions for most efficient and practical OPG performance while taking into account LIDT of the crystal (measured LIDT of MgO:PPLN was ~5 J/cm^2 for 400 ps pulses at 1064 nm wavelength). Sharper focusing of the pump beam (smaller confocal parameter, ξ>0.7) resulted in decreased signal wave average power and efficiency. On the other hand, high signal output powers of 95 – 143 mW with slightly lower conversion efficiencies (16.7 – 17.8 %) can be achieved by defocusing the pump beam (ξ<<1) since the whole power from the microlaser can be used. Therefore, optimal ξ=0.7 value exists for which one can achieve highest signal wave conversion efficiency while simultaneously attaining practical output average power level of 23 mW without damaging the crystal. Very clean crystal facets, the use of small pump beam diameters (while maintaining the same intensity), a gradual increase of the pump power (conditioning effect), and the avoidance of translating the crystal at high power operation are the key factors in reducing the risk of the optical damage. Also it should be noted that signal output power (and therefore efficiency) depended on the transverse position of the MgO:PPLN grating with respect to the pump beam. Effect was present for all of the 8 gratings and indicates non-homogeneous periodic poling within the crystal which limits the OPG performance.

4.2. *Wavelength tuning and spectral characteristics*

Broad and continuous wavelength tuning is the distinctive property of the OPG. As opposed to optical parametric oscillators (OPOs), the tuning range of OPG is not limited by the spectral reflectance characteristics of the resonator's mirrors. In MgO:PPLN based OPG, wavelength tuning of signal and idler waves is achieved by changing the period of the grating and the temperature of the crystal. Figure 7(a) shows signal pulse spectral envelope evolution with varying crystal temperature. For all 8 gratings tuning the temperature from 30 to 200 °C leads to continuous tunability for the signal from 1442 to 2128 nm (2128 – 4040 nm for the idler). Total wavelength tuning range is 2598 nm. A comparison of measured signal central wavelength values with numerical simulations (from Fig. 3(a)) are depicted in Fig. 7(b). Experimentally measured wavelength values basically agreed well with the quantum mechanical model except for Λ=30.8

Optics EXPRESS

μm and Λ=31.47 μm gratings at higher temperatures where small deviation of temperature and grating period results in a significant wavelength changes. Potential reasons of such discrepancy could be attributed to limited resolution of the spectrometer (FWHM ~6.5 nm), inconsistency of the actual and set temperature of the MgO:PPLN, accuracy of the grating period evaluation and the Sellmeier coefficients used for the calculations.

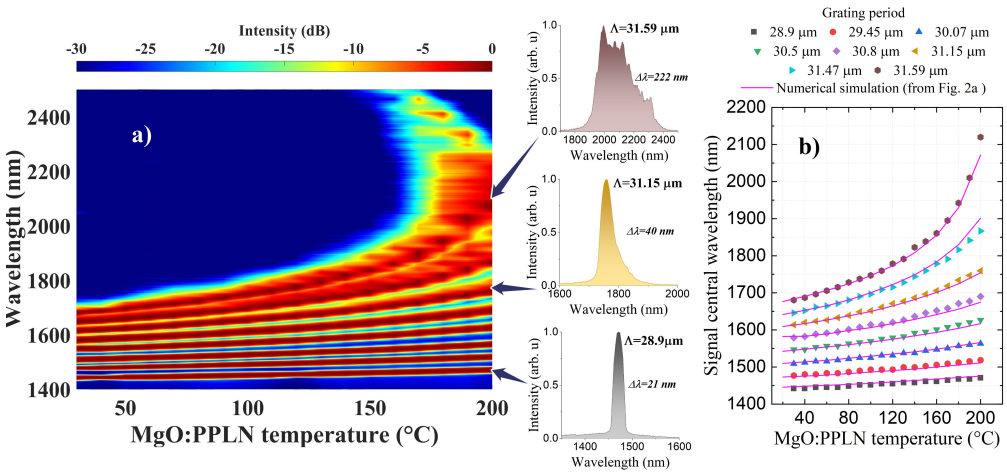

Fig. 7. Signal pulse spectral envelope evolution with varying MgO:PPLN crystal temperature for 8 gratings (a). Additionally, spectra for 3 gratings (Λ=28.9; 31.15; 31.59 μm) is shown at the temperature of 200 °C with corresponding spectral FHWM. (b) – signal central wavelength (dots) vs temperature in comparison with the numerical calculations (solid lines)

Signal wave spectral width (FWHM) increased with the increasing temperature of the crystal and the rise of spectral width was more pronounced for a higher period gratings (due to larger gain bandwidth). For first 7 gratings, Λ=28.9 – 31.47 μm, FHWM ranges from 10 to 62 nm which agrees with the numerical model and denotes signal spectra broadening of more than three orders of magnitude compared to the pump pulse spectrum (≈5 pm FWHM). Figure 7(a) also clearly shows that by tuning the temperature from 150 °C to 200 °C for highest period grating (Λ= 31.59 μm), idler and signal waves approach each other and merge into one very broad degenerate spectrum with FWHM of 222 nm.

4.3. *Signal wave beam quality*

The spatial beam profiles of the output from the OPG at the central wavelength of 1942 nm (Λ=31.59 μm, T = 180 °C) measured using microbolometer camera (WinCamD-IR-BB) is shown in Fig. 8. In the case of sharp pump focusing, the center of the beam is composed of a high-intensity Gaussian distribution and is surrounded by a wide low-intensity peripheral. Beam profile in the X axis (Fig. 8(a)), in fact, reveals that measured beam profile values fit with the Lorentz intensity distribution very well. As a rule, the output beam from the OPG's exhibit high non-diffractive divergence and our case is no exception - signal beam is not diffraction limited as the estimated beam quality parameter M^2 was ~ 2. We also observed that the spatial beam profile depended on the focusing conditions of the pump beam. For a weak pump focusing condition case (Figs. 8(b, c)), beam profile has acquired an ever-widening peripheral as the pump power was increased from 200 mW to 860 mW. At maximum pump power beam profile no longer retains Lorentzian transverse profile (Fig. 8(c)). As a consequence, beam quality parameter M^2 increased from 2.8 at 200 mW pump to 5.4 at maximum pump power. Despite that, ellipticity of the beam in all cases is >0.9. Such deterioration of the beam quality under different focusing

Optics EXPRESS

conditions of the pump could be an indication of non-homogeneous periodic poling of the crystal. To improve the beam quality of the device, a nearly diffraction-limited pump beam should be used and the periodic poling of the crystal must be homogeneous throughout the volume of the grating.

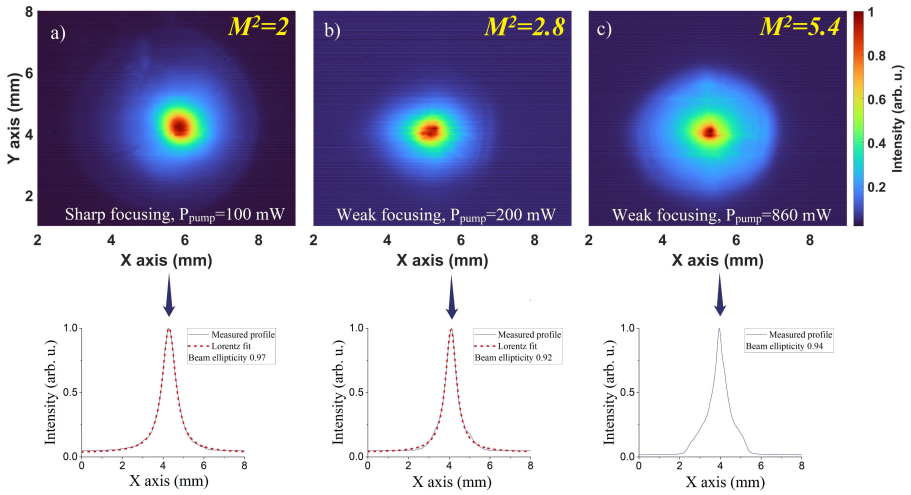

Fig. 8. Spatial beam profile from the OPG for sharp (a) and weak (b, c) pump focusing conditions with corresponding beam profiles in the X axis. Solid blue line – experimental data, dashed red line – Lorentz function fit.

4.4. Temporal properties of the signal wave

Using time-correlated single photon counting technique (TCSPC, PicoHarp 300) we measured temporal properties of the signal pulses. Figure 9(a) shows measured signal pulse temporal FWHM dependence on the pump power at MgO:PPLN temperature of 60 °C for sharp pump focusing case (ξ=0.7). It is evident that there is a pump power at which the minimum signal pulse duration is reached. Above the generation threshold (which is lower for gratings of a higher period), signal pulse width is quickly reduced compared to pump down to 242 – 252 ps (± 16 ps). Shortest pulse duration is achieved just above the generation threshold when the conversion efficiency is low (2 – 5 %) and when the pump is only slightly depleted (Fig. 9(b)). Temporal compression of signal pulse by a factor of ~2 is observed because in 30 – 100 mW pump power range $gL>>1$ and OPG works in the high-gain regime where the signal pulse duration is $\sim\sqrt{gz}^{-1}$ (z is propagation distance in the crystal). As the pump power is further increased, OPG switches to nonlinear regime in which pump pulse intensity is no longer constant, starts to be depleted and signal pulse duration approaches the duration of the pump pulse. At maximum pump power of 100 mW signal pulse FWHM is 405 ps and the leading front of the pulse is slightly steeper than the trailing front due to asymmetrically depleted pump (Fig. 9(b)). Obviously output pulses from the subnanosecond OPG are far from spectrally-limited due to broad output spectra. For example, Λ=29.45 μm grating at 60 °C temperature has a FWHM spectral bandwidth of 17 nm and with temporal FWHM of 405 ps this results in a time-bandwidth product (TPB) of $\Delta\tau\Delta\nu$=927, which is >2000 times the transform-limit for a Gaussian pulse. Analogous regularities of the temporal characteristics of the signal wave were recorded in the case of weak pump focusing (ξ=0.05). Thus, such OPG possesses not only a wide and continuous wavelength tuning range, but also enables the adjustment of the signal pulse duration which could be useful in certain applications. However some of them require nearly transform-limited signal pulses with very narrow spectral

Optics EXPRESS

line - this can be achieved by injection seeding technique which is discussed in the following section.

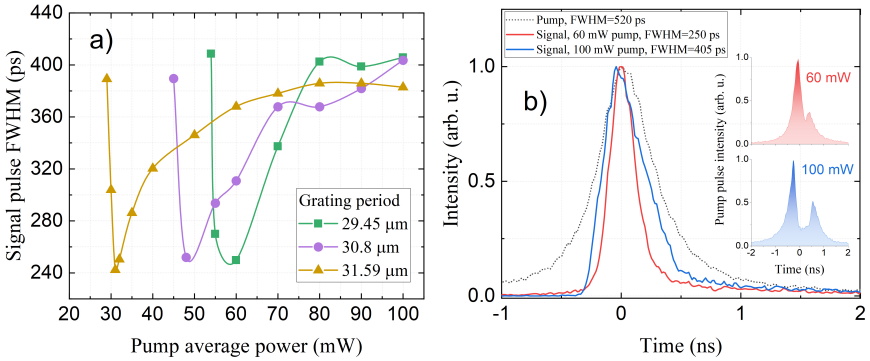

Fig. 9. Signal pulse temporal width vs pump average power for Λ=29.45; 30.8; 31.59 μm gratings (a). Temporal pulse profiles of the pump and signal waves for Λ=29.45 μm grating (b). The inset in (b) shows the depleted pump pulses at 60 mW (red) and 100 mW (blue) pump powers. T = 60 °C. Sharp pump focusing case (ξ=0.7).

5. Subnanosecond OPA in MgO:PPLN

The efficiency of the optical parametric down-conversion process may be enhanced with the use of a coherent light source as a seed. Such technique is called injection seeding and it also allows to narrow OPG signal wave spectrum by orders of magnitude which is necessary for spectroscopy, LIDAR, THz generation, etc. [21]. Here, the quantum mechanical model is redundant and we simulate the optical parametric amplification by the classical three-wave interaction equations in the time and space domains. The governing equations read:

$$\frac{dS_s}{dz} = i(k_s - k_{s0} - \frac{k_r^2}{2k_{s0}})S_s - i\sigma_s FT[A_i^* A_p]\exp(i\Delta kz), \tag{5}$$

$$\frac{dS_i}{dz} = i(k_i - k_{i0} - \frac{k_r^2}{2k_{i0}})S_i - i\sigma_i FT[A_s^* A_p]\exp(i\Delta kz), \tag{6}$$

$$\frac{dS_p}{dz} = i(k_p - k_{p0} - \frac{k_r^2}{2k_{p0}})S_p - i\sigma_p FT[A_s A_i]\exp(-i\Delta kz). \tag{7}$$

Here, $S_j(\Omega, k_r, z)$ are the Fourier transforms of the complex amplitudes $A_j(t, r, z)$, indices $j = s, i, p$ stand for the signal, idler and pump waves, respectively. z and t are the longitudinal propagation distance and time, respectively. $r = \sqrt{x^2 + y^2}$ and (x, y) are the transverse coordinates. First rhs. terms describe the linear propagation, e.g. time walk-off, group velocity dispersion and higher-order dispersion effects as well as beam diffraction, while the second rhs. terms correspond to the nonlinear interaction in the nonlinear crystal. $k_j(\omega) = \omega n_j(\lambda)/c$ is the wavelength-dependent wavenumber of the j-th wave, while k_{j0} is calculated at central wavelength. $\Delta k = k_{p0} - k_{s0} - k_{i0}$ is the phase-mismatch. Nonlinear interaction coefficient $\sigma_j = \pm d_{\text{eff}}\omega_{j0}/(cn_{j0})$ changes its sign every $\Delta z = \Lambda/2$ distance.

Optics EXPRESS

The input complex amplitudes were simulated as follows:

$$A_p(t, z = 0) = a_{p0} \exp\left(-2 \ln 2 \frac{t^2}{\tau_p^2}\right) \exp\left(-\frac{r^2}{r_p^2}\right), \tag{8}$$

$$A_i(t, z = 0) = 0, \tag{9}$$

$$A_s(t, z = 0) = a_{s0} \exp\left(-\frac{r^2}{r_s^2}\right). \tag{10}$$

Therefore, the pump wave is a subnanosecond pulse, the input idler wave is absent and the signal wave corresponds to the DFB CW-mode laser diode. MDL seeder is not described by Eq. (10). a_{p0} and a_{s0} are the pump and signal amplitudes. Pump beam radius r_p is given in Table 1 and seed beam radius $r_s = r_p$. Calculations were done for the fourth grating ($\Lambda = 30.5$ μm) at temperature of $T = 40$ °C because it precisely corresponds to the seed wavelength of $\lambda_{s0} = 1550$ nm. As in OPG case, Sellmeier equation for e→ee interaction formula from [18] was utilized. Equations (5–7) were simulated by the use of the split-step Fourier transform method [22]. The crystal length was divided into $40 \times \text{int}(L/\Lambda)$ longitudinal steps. Here, int(∘) denotes the integer value. The time domain $t \in [-4\tau,\ 4\tau)$ was divided into 256 parts. For the space domain, fast Hankel transform was utilized [23] since the cylindrical symmetry was assumed. The space domain $(0,\ 2r_p]$ was divided into 80 parts.

The comparison of results from numerical simulations and experimental data is presented in Figs. 10 and 11. From experimental signal wave conversion efficiency vs pump power curves (solid lines in Fig. 10(a)) it is seen that by injection seeding the parametric generator with just 0.1 – 1 mW seed power, the 1550 nm wavelength generation threshold is reduced by 15 – 43 % (from 40 mW to 23 – 34 mW) compared to the unseeded OPG. Reduction of the threshold is especially important since the subnanosecond OPG operates not too far from the LIDT of the MgO:PPLN crystal. On the other hand, numerical calculations show sharper increase of conversion efficiencies and signal powers above the generation thresholds which are slightly, 5 – 12 mW, lower than the ones in the experiment. Numerically simulated generation threshold is overestimated due to idealized input signal wave model, Eq. (10) that describes a coherent wave which spectrum is a Dirac delta-function. As the pump power is increased further, experimental conversion efficiency curves start to saturate due to pump depletion. Compared to OPG, signal conversion efficiency throughout the range of pump powers of the OPA is higher by 4 – 20 %. Theoretical calculations predict a few percent higher maximum efficiency that does not roll off at 80 – 100 mW pump range. In numerical simulations, higher saturation values are caused by the idealized coherent input signal wave model, however, theoretical and experimental values agree very well in the 40 – 80 mW pump power range. The M^2 parameter of the signal wave beam from the OPA was very similar to the OPG and measured to be ~2.1. Temporal signal pulse profiles, measured using TCSPC, are shown in the Fig. 10(b) and indicates good agreement between pulse durations obtained from the numerical simulations and experiment, yet the theoretical pulse (that was obtained by integrating over spatial coordinate) has steeper and symmetrical fronts compared to the measured pulse. Nevertheless, output OPA pulses are subnanosecond, shorter than the pump pulse by ≈100 ps and 20 – 60 ps longer than the OPG signal pulses. Although not shown here, the same reduction of the generation threshold, increase in conversion efficiency, and characteristics of the pulse profiles are achieved with multimode CW laser diode (MDL) seed.

From numerical simulations of OPG and OPA signal spectra (Fig. 11(a)) it is seen that by injection seeding the OPG with only 1 mW power narrow linewidth DFB CW diode laser, the signal spectral FWHM is reduced from 17 nm to 11 pm leading to a ~1500 times increase in spectral density. Theory also shows that DFB seed OPA spectra is essentially independent on the pump power (Fig. 11(b)). In contrary to that, OPG signal spectra does depend on the pump power, quickly and symmetrically broadens above the generation threshold and saturates at ≈60

Optics EXPRESS

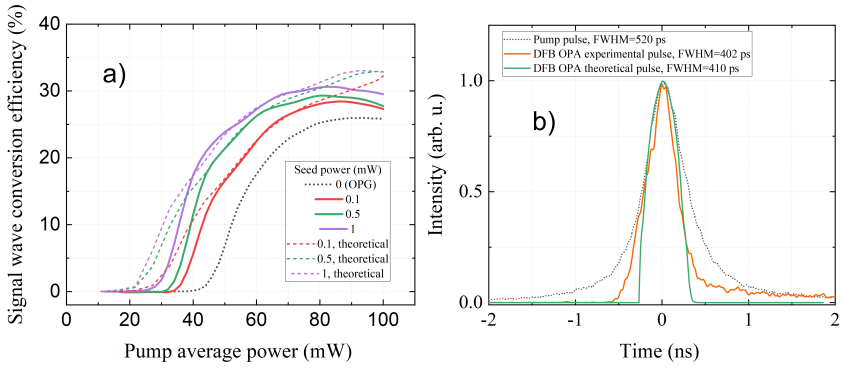

Fig. 10. Signal wave conversion efficiency as a function of pump power in OPA regime for Λ=30.5 μm grating at 0 (OPG case), 0.1, 0.5 and 1 mW DFB seed powers (a). T = 40 °C. Solid lines - OPA experimental data, dotted line - OPG experimental data, dashed lines - results from the numerical calculations. (b) - temporal pulse profiles of the pump (dotted line), experimental (orange solid line) and theoretical (green solid line) signal waves. 70 mW pump power.

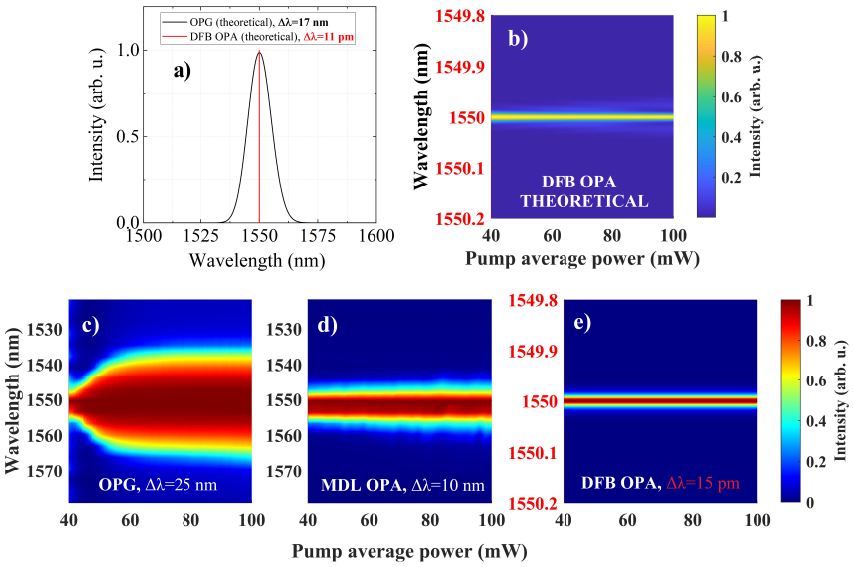

Fig. 11. OPA and OPG signal wave spectra calculated from numerical model at T = 40°C (a). Surface plots shows signal wave spectral envelope evolution with increasing pump power: OPA with DFB seed from numerical simulations (b), experimental OPG (c), experimental OPA with multimode (MDL) seed (d), and experimental OPA with DFB seed (e). Seed power in all cases is 1 mW.

Optics EXPRESS

mW pump power (Fig. 11(c)). Employing MDL seed for injection seeding, the output spectra narrows, however, only by 2.5 times compared to OPG (Fig. 11(d)). Spectral density is increased even further by using DFB seed with a linewidth of <500 kHz. By measuring interference fringe visibility vs optical path distance with a Michelson interferometer, we were able to evaluate the coherence length l_c of the output OPA pulses and calculate the FHWM spectral width given by $\Delta\lambda = \lambda^2/l_c$. Experimental data (Fig. 11(e)) indicate that DFB OPA produces pump power independent very narrow output spectra with $\Delta\lambda \approx 15 - 17$ pm, which agrees very well with the numerical calculations from Fig. 11(a) and (b). The output OPA pulses in 23 – 100 mW pump range are 250 – 420 ps long, therefore TPB of such pulses is in the interval of 0.47 - 0.9 (assuming Gaussian pulse), hence high spectral density, nearly transform-limited subnanosecond OPA pulses are obtained.

6. Summary

In summary, we have presented detailed theoretical and experimental characterization of subnanosecond OPG and OPA based on 20-mm-long MgO:PPLN crystal pumped by a passively Q-switched Nd:YAG micro-laser. Simple, compact, single-pass OPG provided continuous wavelength tunability in 1442 – 4040 nm range with signal wave energies from 33 μJ to 265 μJ. In this work we showed that high OPG conversion efficiencies (up to 46%) even for relatively short-length crystals are possible in subnanosecond pulse duration range without laser damage. Optimal focusing conditions ($\xi = 0.7$) of the pump beam was found for most efficient and practical OPG performance while taking into account LIDT of the crystal. Signal wave exhibits Lorentzian spatial beam profile of with $M^2 \approx 2$ and deteriorates with weaker pump focusing conditions ($M^2 \approx 5.4$) which could indicate distortions and non-homogeneity in the domain structure of the MgO:PPLN crystal. The exponential and nonlinear parametric gain regimes provided by the high nonlinearity and high, up to 2 GW/cm^2 pump intensity in the periodically-poled crystal resulted in a tunable signal pulse duration from 242 to 405 ps. For the first time, the quantum mechanical model for the subnanosecond OPG was adopted. It predicted the signal wave spectra and wavelength tunability with sufficient accuracy, yet the model needs improvements for the calculation of the output power at large gL>10 values. By injection seeding the OPG, the signal generation threshold was reduced up to 1.6 times, maximum conversion efficiency was increased by 4 – 20% and the pulse TBP was significantly improved due to the narrowing of the signal spectrum by more than three orders of magnitude. Good agreement with the OPA theoretical model based on classical three-wave interaction equations was achieved. Low threshold, high-efficiency, tunable, and nearly transform-limited output OPA pulses can be achieved by implementing narrow-band DFB CW seeders throughout the signal tuning range. Combined with additional frequency conversion stages wavelength tuning could be extended to visible and UV regions. Potential low cost and simple design of subnanosecond microchip parametric devices makes them attractive for variety of applications that require pulsed and tunable wavelength laser light.

Funding. Lietuvos Mokslo Taryba (No. 01.2.2-LMT-K-718-03- 0004).

Acknowledgments. This work has received funding from European Regional Development Fund (project No. 01.2.2-LMT-K-718-03-0004) under grant agreement with the Research Council of Lithuania (LMTLT). We would like to thank Mikas Vengris (Vilnius University) for providing time-correlated single photon counting system, Rytis Butkus (Vilnius University) for lending the microbolometer camera and for Julianas Želudevičius (Center for Physical Sciences and Technology) for providing the DFB diode laser.

Disclosures. The authors declare no conflicts of interest.

Data availability. Data underlying the results presented in this paper are not publicly available at this time but may be obtained from the authors upon reasonable request.

References

Optics EXPRESS

1. G. W. Baxter, M. A. Payne, B. D. W. Austin, C. A. Halloway, J. G. Haub, Y. He, A. P. Milce, J. F. Nibler, and B. J. Orr, "Spectroscopic diagnostics of chemical processes: applications of tunable optical parametric oscillators," Appl. Phys. B **71**(5), 651–663 (2000).
2. M. Hori, H. Aghai-Khozani, A. Sótér, A. Dax, and D. Barna, "Laser spectroscopy of pionic helium atoms," Nature **581**(7806), 37–41 (2020).
3. Y. Takida, T. Ikeo, K. Nawata, Y. Wada, Y. Higashi, and H. Minamide, "Terahertz differential absorption spectroscopy using multifurcated subnanosecond microchip laser," Appl. Phys. Lett. **115**(12), 121102 (2019).
4. S. Lambert-Girard, M. Allard, M. Piché, and F. Babin, "Broadband and tunable optical parametric generator for remote detection of gas molecules in the short and mid-infrared," Appl. Opt. **54**(10), 2594–2605 (2015).
5. Y. Jiang, J. Yang, P. Li, H. Si, X. Fu, and Q. Liu, "High energy lidar source for long distance, high resolution range imaging," Microw. Opt. Technol. Lett. **62**(12), 3655–3661 (2020).
6. M. Laroche, P. Leproux, V. Couderc, C. Lesvigne, H. Gilles, and S. Girard, "Compact sub-nanosecond wideband laser source for biological applications," Appl. Phys. B **86**(4), 601–604 (2007).
7. S. L. Genc, H. Ma, and V. Venugopalan, "Low-density plasma formation in aqueous biological media using sub-nanosecond laser pulses," Appl. Phys. Lett. **105**(6), 063701 (2014).
8. K. Nawata, T. Notake, H. Ishizuki, F. Qi, Y. Takida, S. Fan, S. Hayashi, T. Taira, and H. Minamide, "Effective terahertz-to-near-infrared photon conversion in slant-stripe-type periodically poled linbo3," Appl. Phys. Lett. **104**(9), 091125 (2014).
9. M. M. Fejer, G. A. Magel, D. H. Jundt, and R. L. Byer, "Quasi-phase-matched second harmonic generation: tuning and tolerances," IEEE J. Quantum Electron. **28**(11), 2631–2654 (1992).
10. J. J. Zayhowski, "Periodically poled lithium niobate optical parametric amplifiers pumped by high-power passively q-switched microchip lasers," Opt. Lett. **22**(3), 169–171 (1997).
11. A. C. Chiang, Y. C. Huang, Y. W. Fang, and Y. H. Chen, "Compact, 220-ps visible laser employing single-pass, cascaded frequency conversion in monolithic periodically poled lithium niobate," Opt. Lett. **26**(2), 66–68 (2001).
12. H. Ishizuki and T. Taira, "High-gain mid-infrared optical-parametric generation pumped by microchip laser," Opt. Express **24**(2), 1046–1052 (2016).
13. J. Yue, T. Tamada, M. Kamata, L. Zheng, H. Ishizuki, and T. Taira, ">2 MW peak power at 1560 nm from micro giant-pulse laser/amplifier with PPMgLN OPG," in *Lasers Congress 2016 (ASSL, LSC, LAC)*, (OSA, Washington, D.C., 2016).
14. L. Liu, H. Y. Wang, Y. Ning, C. Shen, L. Si, Y. Yang, Q. L. Bao, and G. Ren, "Sub-nanosecond periodically poled lithium niobate optical parametric generator and amplifier pumped by an actively q-switched diode-pumped Nd:YAG microlaser," Laser Phys. **27**(5), 055403 (2017).
15. H. Qiao, K. Zhong, F. Li, X. Zhang, Q. Sheng, W. Shi, D. Xu, and J. Yao, "High-peak-power, high-efficiency, widely tunable sub-nanosecond optical parametric generator based on PPMgLN," in *Quantum and Nonlinear Optics VIII*, Q. He, C.-F. Li, and D.-S. Kim, eds. (SPIE, 2021).
16. K. Zhong, H. Qiao, F. Li, X. Zhang, Y. Zheng, S. Wang, D. Xu, and J. Yao, "Tunable narrow-linewidth high-peak-power sub-nanosecond optical parametric generator by injection seeding," Opt. Express **30**(10), 16479–16488 (2022).
17. S. Acco, P. Blau, and A. Arie, "Output power and spectrum of optical parametric generator in the superfluorescent regime," Opt. Lett. **33**(11), 1264–1266 (2008).
18. O. Paul, A. Quosig, T. Bauer, M. Nittmann, J. Bartschke, G. Anstett, and J. A. L'Huillier, "Temperature-dependent Sellmeier equation in the MIR for the extraordinary refractive index of 5% MgO doped congruent $LiNbO_3$," Appl. Phys. B **86**(1), 111–115 (2006).
19. A. P. Piskarskas, A. P. Stabinis, and V. Pyragaite, "Ultrabroad bandwidth of optical parametric amplifiers," IEEE J. Quantum Electron. **46**(7), 1031–1038 (2010).
20. G. Boyd and D. Kleinman, "Parametric interaction of focused gaussian light beams," J. Appl. Phys. **39**(8), 3597–3639 (1968).
21. B. Dolasinski, P. E. Powers, J. W. Haus, and A. Cooney, "Tunable narrow band difference frequency thz wave generation in dast via dual seed ppln opg," Opt. Express **23**(3), 3669–3680 (2015).
22. M. S. Wartak, *Computational Photonics: An Introduction with MATLAB* (Cambridge University Press, United Kingdom, 2013).
23. P. P. Banerjee, G. Nehmetallah, and M. R. Chatterjee, "Numerical modeling of cylindrically symmetric nonlinear self-focusing using an adaptive fast hankel split-step method," Opt. Commun. **249**(1-3), 293–300 (2005).